Negatively Charged Metal Oxide Nanoparticles Interact with the 20S Proteasome and Differentially Modulate Its Biologic Functional Effects

Christine A. Falaschetti,[†] Tatjana Paunesku,[†] Jasmina Kurepa,[‡] Dhaval Nanavati,[§] Stanley S. Chou,[⊥] Mrinmoy De,[⊥] MinHa Song,[∥] Jung-tak Jang,[∥] Aiguo Wu,[¶] Vinayak P. Dravid,[⊥] Jinwoo Cheon,[∥] Jan Smalle,[‡] and Gayle E. Woloschak[†,*]

[†]Feinberg School of Medicine, Department of Radiation Oncology, Northwestern University, Chicago, Illinois 60611, United States, [‡]Department of Plant and Soil Sciences, University of Kentucky, Lexington, Kentucky 40546, United States, [§]Chemistry of Life Processes Institute, Proteomics Core, Northwestern University, Evanston, Illinois 60208, United States, [⊥]Department of Materials Science and Engineering, Northwestern University, Evanston, Illinois 60208, United States, [∥]Department of Chemistry, Yonsei University, Seoul 120-749, South Korea, and [¶]Division of Functional Materials and Nano-Devices, Ningbo Institute of Materials Technology & Engineering, Ningbo 315201, China

ABSTRACT The multicatalytic ubiquitin–proteasome system (UPS) carries out proteolysis in a highly orchestrated way and regulates a large number of cellular processes. Deregulation of the UPS in many disorders has been documented. In some cases, such as carcinogenesis, elevated proteasome activity has been implicated in disease development, while the etiology of other diseases, such as neurodegeneration, includes decreased UPS activity. Therefore, agents that alter proteasome activity could suppress as well as enhance a multitude of diseases. Metal oxide nanoparticles, often developed as diagnostic tools, have not previously been tested as modulators of proteasome activity. Here, several types of metal oxide nanoparticles were found to adsorb to the proteasome and show variable preferential binding for particular proteasome subunits with several peptide binding "hotspots" possible. These interactions depend on the size, charge, and concentration of the nanoparticles and affect proteasome activity in a time-dependent manner. Should metal oxide nanoparticles increase proteasome activity in cells, as they do *in vitro*, unintended effects related to changes in proteasome function can be expected.

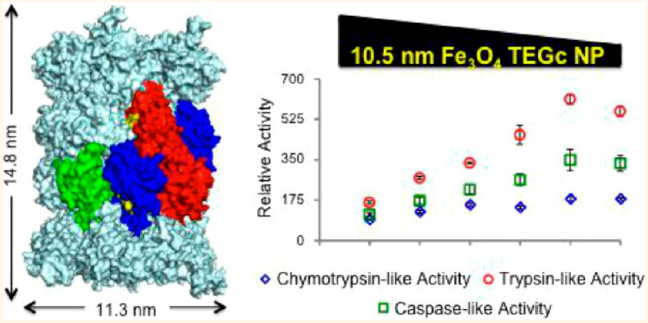

KEYWORDS: iron oxide nanoparticles · titanium dioxide nanoparticles · protein adsorption · ubiquitin–proteasome system · proteasome activation

The ubiquitin–proteasome system (UPS) is conserved in all eukaryotic species and is responsible for the timely and orderly degradation of the majority of cellular proteins, regulating in that way most cellular processes.[1−3] To maintain cellular homeostasis, the UPS targets not only misfolded and oxidized proteins but also cyclins, DNA repair proteins, and apoptosis proteins when their presence interferes with the ongoing cellular events.[4] Polyubiquitination most often triggers proteolysis, and ubiquitin modification is carried out by ubiquitin-activating (E1), ubiquitin-conjugating (E2), and ubiquitin–protein ligase (E3) enzymes.[5,6]

Protein degradation is executed by the 26S proteasome, which receives and processes poly-ubiquitinated proteins. Two subcomplexes complete the 26S proteasome: the 28-subunit core particle (20S proteasome) and the 19-subunit regulatory particle (19S proteasome).[7,8] The 20S proteasome is a stable protein complex, barrel-shaped, and composed of four stacked heptameric rings of α and β subunits arranged as $\alpha_{1-7}\beta_{1-7}\beta_{1-7}\alpha_{1-7}$.[9] The two outer rings are composed of proteolytically inactive α subunits forming a narrow pore that allows entrance of unfolded substrate proteins into the inner space of the complex, the proteolytic chamber. The active sites of

* Address correspondence to g-woloschak@northwestern.edu.

Received for review May 13, 2013 and accepted August 9, 2013.

Published online August 09, 2013
10.1021/nn402416h

TABLE 1. Summary of the Nanoparticles Used in This Work[a]

chemical composition	average diameter (nm)	hydrodynamic diameter (nm)	surface area per mol (nm^2/mol)	shape	surface coating	zeta-potential (mV)	fwhm (mV)
Fe_3O_4	10.5 ± 1.1	42.6 ± 1.3	2.1×10^{26}	sphere	TEGc[b]	−54 ± 1	21 ± 1
Fe_3O_4	10.5 ± 1.1	43.6 ± 0.8	2.1×10^{26}	sphere	PEG600c[c]	−76 ± 3	26 ± 3
Fe_3O_4	4.1 ± 0.6	31.2 ± 0.7	3.3×10^{25}	sphere	TEGc	−36 ± 1	18 ± 2
Fe_3O_4	4.1 ± 0.6	27.1 ± 1.1	3.3×10^{25}	sphere	PEG600c	−31 ± 1	27 ± 3
TiO_2	20.2 × 3.0 ± 4.4 × 0.2	N/A	1.2×10^{26}	rod	OH[d]	−64 ± 1	19 ± 1
TiO_2	5.1 × 2.8 ± 1.4 × 0.1	N/A	3.7×10^{25}	rod	OH	−51 ± 6	14 ± 2
Fe_3O_4/Fe_2O_3[e]	∼35	59.5 ± 1.2	2.3×10^{27}	sphere	carboxydextran[f]	−24 ± 1	21 ± 1

[a] Measurements shown here were done in nanopure H_2O; additional zeta-potential measurements in other buffers and in the presence or absence of proteasome 20S complex are given in Supporting Information Table S1. [b] TEGc: tetraethylene glycol-carboxylate (average M_n 250). [c] PEG600c: polyethylene glycol-carboxylate (average M_n 600). [d] Hydroxyl groups are formed as an outcome of tetramethylammonium hydroxide treatment following nanorod synthesis.[49] [e] FeraSpin R, purchased from Miltenyi Biotec. [f] Average MW 70 000.

the β1, β2, and β5 subunits face this inner space and exhibit caspase-, trypsin-, and chymotrypsin-like activity, respectively.[10] The 19S proteasome, an allosteric stimulator of 20S proteolytic activity, recognizes polyubiquitinated proteins, removes ubiquitin moieties, and unfolds substrates to be degraded by the 20S proteasome.[11−14]

In organisms from yeast to humans, activity of the UPS regulates cell cycle progression, signal transduction, and differentiation.[15,16] Diseases as varied as cardiac dysfunction, autoimmune disorders, and viral infections often involve deregulated proteasome activity or expression.[17−19] A decline of proteasome activity often correlates with the appearance of protein aggregates in age-related neurodegenerative diseases.[20−22] In addition, many cancers are linked with increased polyubiquitination and/or proteasome quantity or activity.[23−25]

The investigation of nanomaterials as diagnostic and therapeutic agents in medicine is expanding exponentially. Therefore, it is important to evaluate interactions of nanoparticles with different cellular components and biomolecules.[26] In most biological environments, nanomaterials have the opportunity to interact with local proteins. This leads to the creation of a protein corona, which alters the biological identity of the nanoparticles and modulates biological responses to nanomaterials.[27−30] On the other hand, the folding and activity of the bound proteins often change, as well.[31,32]

Most previous studies on protein coronas have focused on plasma proteins that interact with the nanomaterial rather than on intracellular proteins.[33−36] Among intracellular proteins, the proteasome is present in high concentrations;[37,38] therefore, intracellular contact between nanoparticles and the 20S proteasome complex is likely. A recent study indicated the presence of 20S proteasome subunits in nanoparticle coronas,[39] but the functional effects of these interactions still await full exploration.

Nanoparticles made of gold, iron oxide, and titanium dioxide are among the most abundantly used metallic nanomaterials. Nevertheless, protein interaction studies for the latter two nanoparticle types lag behind work done on Au nanomaterials. For example, a literature search for nanoparticle−protein corona articles published this year results in only one paper on iron oxide, while there are four such articles on Au nanoparticles.[40−44] For work presented here, we assembled a small collection of Fe_3O_4 and TiO_2 nanoparticles (Table 1, Supporting Information Figure S1). Nanoparticle size and shape have been shown to influence interactions with proteins;[45,46] therefore, we selected spherical 4.1 and 10.5 nm Fe_3O_4 nanoparticles as well as FeraSpinR, commercially available nanoparticles with a spherical 35 nm iron oxide core and rod-shaped 20.2 × 3 and 5.1 × 2.8 nm TiO_2 nanoparticles. While large iron oxide nanoparticles such as FeraSpinR found their place in *in vivo* studies as magnetic resonance contrast agents, smaller Fe_3O_4 and Fe_2O_3 nanoparticles are used in different non-MR applications, as well, such as gene delivery.[47] With regard to TiO_2 nanoparticles, rod-shaped nanoparticles were selected because their synthesis allows for a more controlled, monodisperse preparation.[48] All of these nanoparticles were prepared as monodisperse and surface modified with hydroxyl groups or carboxyl groups carried by ethylene glycol or dextran (Table 1). Zeta-potential measurements of these nanoparticles in H_2O and other buffers used in this study, in the presence and absence of the 20S proteasome, are shown in Table 1 and Supporting Information Table S1.

Several approaches were used to evaluate the interactions between selected nanoparticles and the 20S proteasome complex (Figure 1). We investigated the depletion of individual 20S proteasome subunits and their component peptides using Western blot and mass spectrometry. We also studied fluctuations of the 20S proteasome proteolytic activities in the presence of nanoparticles.

RESULTS AND DISCUSSION

Interaction between the 20S proteasome as a whole and nanoparticles was investigated by mixing the 20S proteasome with 10.5 nm Fe_3O_4 nanoparticles coated with tetraethylene glycol-carboxylate (TEGc). These

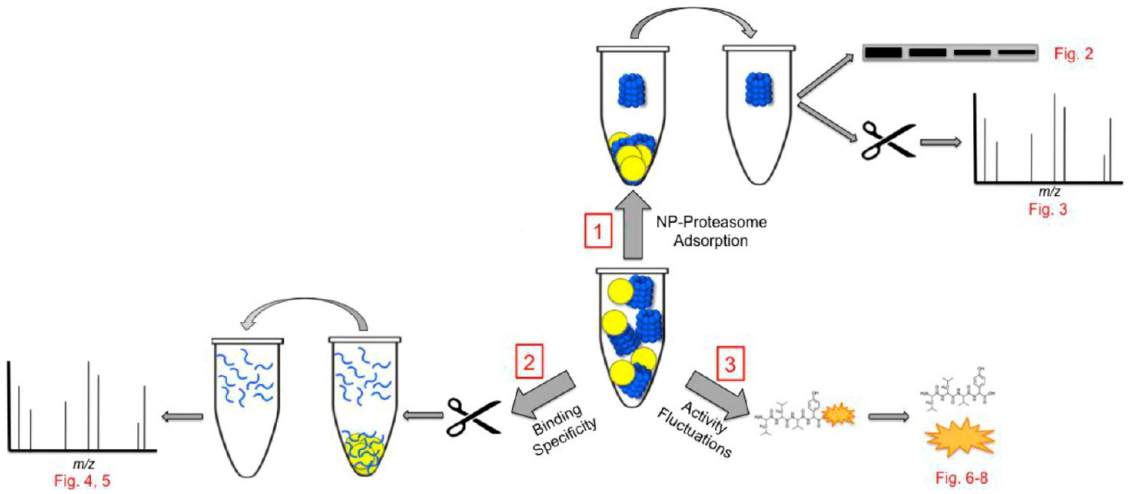

Figure 1. Schematic representation of experimental design. Metal oxide nanoparticles (1) adsorb to the 20S proteasome, (2) show preferential adsorption to several peptide sequences, and (3) induce fluctuations in 20S proteasome activity. (1) Following co-incubation of nanoparticles and 20S proteasome complexes, nanoparticles were pelleted, and unbound 20S proteasome was quantified by Western blot and mass spectrometry (Figures 2 and 3). (2) 20S proteasome co-incubated with nanoparticles was digested either by trypsin, chymotrypsin, or Asp-N; the nanoparticles were subsequently pelleted, and free peptides were analyzed by mass spectrometry (Figures 4 and 5). (3) Cleavable luminogenic peptides were used to evaluate three major catalytic activities of the 20S proteasome in the presence of nanoparticles (Figures 6–8).

"super-complexes" made of nanoparticles and the 20S proteasome were visualized with transmission electron microscopy (Supporting Information Figure S2). Co-incubated nanoparticles and the 20S proteasome were applied to grids, stained with uranyl acetate, and dried. Imaged samples show an interspersed distribution of the 20S proteasome and nanoparticles, suggesting that the nanoparticles preferentially interact with the 20S proteasome rather than with each other.

Next, the 20S proteasome was co-incubated with increasing concentrations of 10.5 and 4.1 nm Fe_3O_4 nanoparticles coated with TEGc or polyethylene glycol-carboxylate (PEG600c). In these experiments, the concentration of proteasome was constant at 440 nM (2 μg of purified 20S proteasome). After 17 h incubations, nanoparticles were pelleted together with the adsorbed 20S proteasome complex. Because of the high colloidal stability of these nanoparticles, it was necessary to induce flocculation before centrifugation. This was done with the addition of 4.5 M NaCl; nanoparticles precipitated in this manner formed an insoluble pellet together with the 20S proteosome complexes adsorbed on their surfaces. The same experimental conditions applied to the 20S proteasome did not lead to free protein precipitation (Supporting Information Figure S3). Next, the supernatant was desalted and 20S proteasome subunits were resolved by SDS-PAGE. The α2 subunit was assessed by a Western blot as a representative protein for the 20S proteasome complex.

In this assay setup, where irreversible co-precipitation of nanoparticles and proteins is obtained after centrifugation, greater adsorption of protein to the nanoparticles corresponds to a reduction in the presence of protein in the supernatant. Using a Western blot for the α2 subunit, we found that the nanoparticles adsorb the 20S proteasome in a concentration-dependent manner (Figure 2). Both 62.3 and 103.8 nM concentrations of 10.5 nm Fe_3O_4 TEGc and PEG600c nanoparticles measurably depleted the α2 20S proteasome subunit from the samples (Figure 2a,d). Only a 600 nM concentration of 4.1 nm Fe_3O_4 TEGc nanoparticles achieved similar levels of 20S proteasome adsorption (Figure 2b,c). The nanoparticle surface area per mol is very different for these two nanomaterials, and the cumulative surface of 103.8 nM 10.5 nm Fe_3O_4 TEGc nanoparticles and 600 nM 4.1 nm Fe_3O_4 TEGc nanoparticles is almost equal at 1.3×10^{16} and 1.2×10^{16} nm^2, respectively. Therefore, it is likely that surface area plays a significant role in the concentration-dependent nanoparticle–20S proteasome binding. However, nanoparticles of different diameters covered with PEG600c did not show a similar result (Figure 2d–f). Due to its greater length and higher polarity, the PEG600c coating may make a greater contribution to the overall nanomaterial properties than TEGc. However, it is difficult to speculate why the binding capacity of 10.5 nm PEG600c particles would be increased and that of 4.1 nm PEG600c particles would be decreased, compared to their TEGc-covered counterparts.

Because the use of high salt concentration and the pelleting step can potentially disrupt nanoparticle–protein interactions,[35] surface plasmon resonance (SPR) was used to confirm the adsorption between nanoparticles and the 20S proteasome (Supporting Information Figure S4). The 20S proteasome was immobilized to carboxyl-coated SPR substrate chips *via* amine-coupling chemistry and exposed to nanoparticles. The 10.5 nm Fe_3O_4 PEG600c nanoparticles demonstrated the highest adsorption capability, while the 4.1 nm Fe_3O_4 PEG600c nanoparticles bound to 20S

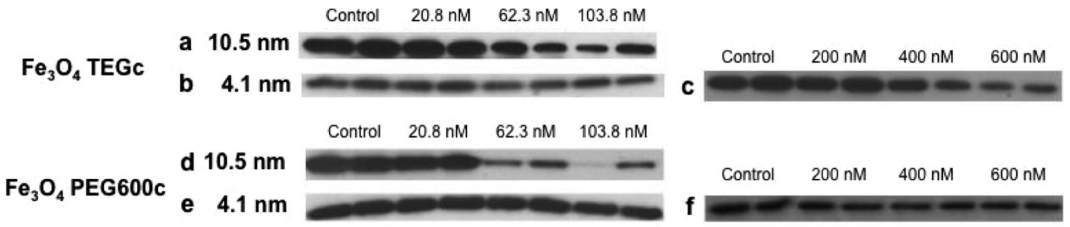

Figure 2. 20S proteasome adsorption to Fe_3O_4 nanoparticles determined through depletion of the α2 subunit. "Free" α2 subunit was quantified by Western blot following a 17 h incubation of 440 nM 20S proteasome with (a) 10.5 nm Fe_3O_4 TEGc, (b, c) 4.1 nm Fe_3O_4 TEGc, (d) 10.5 nm Fe_3O_4 PEG600c, and (e,f) 4.1 nm Fe_3O_4 PEG600c nanoparticles. Nanoparticles and the adsorbed 20S proteasome were irreversibly pelleted in the presence of 4.5 M NaCl and removed from the samples; the α2 subunit remaining in solution was detected by Western blot. Duplicate samples per nanoparticle concentration are presented.

proteasome complexes most weakly (Supporting Information Figure S4). SPR data predicted a nanoparticle/protein stoichiometry greater than 1:1, making it impossible to obtain accurate kinetic parameters for these interactions. These findings were in keeping with the observations made by TEM (Supporting Information Figure S2), which suggested that more than one nanoparticle can interact with a single 20S proteasome complex and *vice versa*.

To determine the adsorption for each of the 20S proteasome subunits individually, we examined the supernatants of nanoparticle−20S proteasome co-incubation experiments by label-free quantification by mass spectrometry (Figure 3). Once again, 10.5 nm Fe_3O_4 TEGc nanoparticles at 20.8 and 103.8 nM concentrations were incubated with 2 μg of 20S proteasome protein (proteasome concentration of 440 nM) for 17 h. The "super-complex" formed from nanoparticles and the 20S proteasome was precipitated by the addition of salt and centrifugation, and the unbound protein in the supernatant was collected. The unbound 20S proteasome was denatured, digested with trypsin, and analyzed by mass spectrometry. Total spectral counting of each subunit in the 20S proteasome was used to measure quantitative difference between nanoparticle-treated 20S proteasome complexes and controls (Figure 3). The spectral counting relies on a general correlation between the number of peptides sequenced per protein and the amount of sample protein. In this experiment, incubation with 20.8 nM 10.5 nm Fe_3O_4 TEGc nanoparticles (nanoparticle/protein ratio of 1:21) does not lead to significant removal of the 20S proteasome; however, incubation with 103.8 nM 10.5 nm Fe_3O_4 TEGc nanoparticles (nanoparticle/protein ratio of 1:4) reduces the quantity of each of the 20S proteasome subunits in the supernatant to close to 40% (Figure 3). A similar degree of depletion of each of the subunits under these experimental conditions suggests that intact 20S proteasome complexes are pulled down by the nanoparticles and that adsorption of the 20S proteasome complex to nanoparticles does not result in subunit dissociation.

To confirm that co-incubation with nanoparticles does not separate the subunits of the 20S proteasome

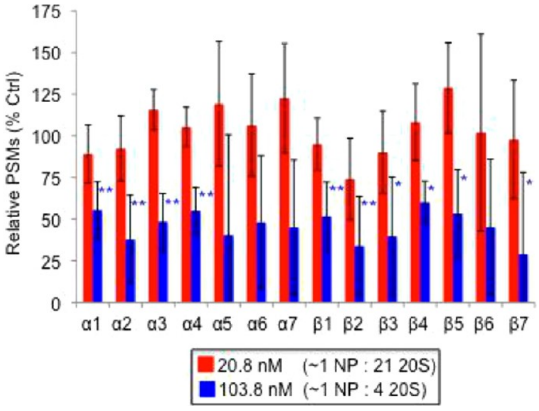

Figure 3. Mass spectrometry analysis of unbound 20S proteasome subunits following co-precipitation of the 20S proteasome and 10.5 nm Fe_3O_4 TEGc nanoparticles. 20.8 nM (red) and 103.8 nM (blue) 10.5 nm Fe_3O_4 TEGc nanoparticles were incubated with the 20S proteasome (440 nM) for 17 h and the adsorbed 20S and nanoparticles irreversibly precipitated. Unbound protein from the supernatant was trypsin digested; peptide spectral matches (PSMs) of each of the 20S proteasome subunits were compared with the nanoparticle-free control. The standard error of triplicate experiments is shown. Statistical significance between experimental and control samples was assessed with an unpaired *t* test, where * reflects a *p* value <0.05 and ** reflects a *p* value <0.01.

or markedly alter the 20S proteasome complex structure, we measured the circular dichroism (CD) spectra of co-incubated mixtures. The 10.5 nm Fe_3O_4 TEGc nanoparticles and the 20S proteasome were co-incubated for 1 min, 3 h, and 17 h (Supporting Information Figure S5). Minimal differences in the spectra could be seen, although a small change in the spectra shape around 220 nm can be noted for the 3 and 17 h incubation time points, possibly indicating a mild change in quantity of α-helix structure in the 20S proteasome.[50]

Although these data suggested that the whole 20S proteasome complex is pulled down by the pelleting of nanoparticles, we wanted to establish if there is a preferential binding between specific 20S proteasome subunits and nanoparticles. To investigate this question, we performed a tryptic digest on a co-incubation mixture of the 20S proteasome and nanoparticles. Similar to before, the nanoparticles and the peptides

still attached to the particle surface were pelleted together, and the non-nanoparticle-bound peptides were analyzed by mass spectrometry (see the schematic diagram in Figure 1). Protein cleavage by trypsin should be hindered close to a nanoparticle's surface; in effect, nanoparticle proximity can be expected to protect the peptides with the trypsin recognition sequence (arginine or lysine followed by an amino acid other than proline).[51] Thus, should any selectivity in interaction between nanoparticles and each of the 20S proteasome subunits exist, the subunits with the strongest binding preference for nanoparticles would be represented by the fewest mass spectrometry-detected peptides.

In this experiment, most of the 20S proteasome subunits after co-incubation with nanoparticles showed decreases in the proportion of full-length amino acid sequences detected (coverage), compared to the coverage of trypsin digested control 20S proteasome (Figure 4). While this effect was concentration-dependent, protein coverage losses induced by the 103.8 nM nanoparticle treatment were more frequently statistically significant than those found after co-incubation with 20.8 nM nanoparticles. Additionally, the most striking depletion affected the β6 and β7 subunits, indicating that their binding to the 10.5 nm Fe_3O_4 TEGc nanoparticles is the most prominent (Figure 4). According to the crystal structure of the mammalian 20S proteasome, the two β6 and the two β7 subunits are in close proximity to one another.[52] Therefore, it is possible that one nanoparticle can interact with more than one of these subunits at the same time.

Because of the presence of carboxyl groups in the TEGc and PEG600c molecules, nanoparticle surfaces of TEGc and PEG600c nanoconstructs could be expected to form ionic interactions with basic amino acid residues such as arginine and lysine. To investigate whether the peptides most firmly bound to the nanoparticles have an unusual number of these amino acids, we screened the peptide sequences present and absent in peptide mixtures obtained from co-incubation−digestion−precipitation experiments similar to that described in Figure 4. Different concentrations of 10.5 nm Fe_3O_4 TEGc nanoparticles were used varying the nanoparticle/protein ratio from 1:50 to 2:1 (Table 2, Figure 5, and Supporting Information Figures S6, S7 and Tables S2, S3), and the protein−nanoparticle complexes were digested by trypsin before nanoparticle precipitation. In addition, 20S proteasome incubated with 10.5 nm Fe_3O_4 TEGc nanoparticles at a nanoparticle/protein ratio of 1:4 was also digested with chymotrypsin or with endoproteinase Asp-N (Table 2, Figure 5, and Supporting Information Figure S7). Because cleavage sequences for these three endopeptidases differ, we decided that the most "conservative" evaluation of nanoparticle-adsorbed peptides from the 20S proteasome should be limited to peptides absent from the reaction supernatant of all three digests.

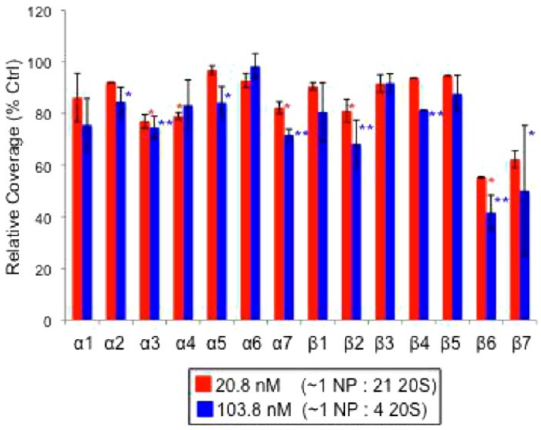

Figure 4. Mass spectrometry analysis of the peptides of each 20S proteasome subunit not engaged in binding with 10.5 nm Fe_3O_4 TEGc nanoparticles. 440 nM 20S proteasome incubated with 20.8 nM (red) and 103.8 nM (blue) nanoparticles for 17 h was trypsin digested in the presence of the nanoparticles. Nanoparticles were then precipitated from the samples, and non-nanoparticle-bound peptides were analyzed by mass spectrometry. Protein coverage, the fraction of each full-length amino acid protein sequence determined by mass spectrometry, is altered for majority of the 20S proteasome subunits. Loss of protein coverage is more pronounced with higher nanoparticle concentrations. Standard error of triplicate samples is shown. Statistical significance was assessed with an unpaired *t* test, where * reflects a *p* value <0.05 and ** reflects a *p* value <0.01.

Sequences of these peptides are provided in Table 2 and underlined in Supporting Information Figure S6. Positions of these peptides have been superimposed on the 3D structure of the 20S proteasome in Figure 5 and Supporting Information Figure S7. 20S proteasome amino acid sequences not detected by mass spectrometry following incubation with other types of nanoparticles (10.5 nm Fe_3O_4 PEG600c, 4.1 nm Fe_3O_4 TEGc, and 4.1 nm Fe_3O_4 PEG600c) at a 1:1 nanoparticle/protein ratio are also shown in Supporting Information Table S3.

Each of the peptides protected from proteolysis by interaction with the nanoparticles is situated on the external surface of the 20S proteasome, consistent with the idea that 10.5 nm Fe_3O_4 TEGc nanoparticles should be prevented from penetrating the considerably smaller entrance pore of the 20S proteasome (~1.3 nm).[9] As reflected in Figure 4, subunits β6 and β7 show particularly long amino acid binding stretches (Table 2). Working with a cellular extract, Lundqvist and others found β5 and β6 proteasome subunits in the protein corona of silica nanoparticles.[39] However, since these researchers did not focus on specific amino acid interactions with their nanoparticles, it is difficult to speculate whether the 20S proteasome peptides responsible for nanoparticle adsorption in that study are identical to those identified here.

Inspection of Table 2 suggests that no specific amino acid sequence or even single amino acid shows up more frequently than the others in this set of peptides. The only apparent similarity between these peptides is that in each case the most polar amino acid of the

TABLE 2. Identities of 20S Proteasome Peptides Adsorbing Most Strongly to 10.5 nm Fe_3O_4 TEGc Nanoparticles[a]

subunit	nanoparticle-bound peptide	mass (Da)	pI	net charge pH 7.6	net charge pH 8.0	hydrophilic ratio	polarity (Zimmerman) (min, max)	average area buried (min, max)
α1	RPYGVGL	760.9	9.8	0.7	0.5	0.14	0.043, 18.397	88.933, 144.267
α3	DIVKEVAK	901.1	7.0	−0.3	−0.5	0.50	16.543, 33.177	113.833, 138.167
	ELELSWVGELTNGR	1602.8	4.0	−2.3	−2.5	0.43	0.743, 33.310	90.900, 158.100
	DIREEAEKYAK	1351.5	4.7	−1.3	−1.5	0.64	17.037, 50.600	104.800, 144.700
α4	VLNKTMDVSK	1134.4	9.9	0.7	0.5	0.50	1.213, 18.180	108.133, 137.233
α6	TQNAEMRPL	1059.2	70	−0.3	−0.5	0.44	2.303, 34.443	101.267, 149.667
α7	RPFGISALIVGFDFDGTPR	2065.4	6.9	−0.3	−0.5	0.26	0.087, 33.250	87.433, 162.000
β2	DYLAALAK	864.0	6.7	−0.3	−0.5	0.25	0.043, 17.147	112.433, 146.533
β5	VIEINPY	847.0	3.3	−1.3	−1.5	0.29	1.697, 17.803	118.067, 143.300
β6	QLGFHSIELNEPPLVHTAASLFK	2548.9	6.0	−1.1	−1.4	0.30	0.160, 18.287	86.267, 157.900
	SVPMGGMMVRQSFAIGGGSGSYIYGYVDATYR	3465.9	9.3	0.7	0.5	0.27	0.000, 19.067	62.900, 171.133
β7	LISSNLELHSLSTGR	1626.8	7.9	−0.2	−0.5	0.47	0.643, 33.877	85.000, 147.367
	MLKQMLFR	1066.4	11.5	1.7	1.5	0.38	0.637, 18.153	132.933, 177.033

[a] The hydrophilic ratio corresponds to the number of hydrophilic residues, as compared to the total number of residues. Each peptide's polarity (Zimmerman values) and the scale for "average area buried on transfer from standard state to folded protein" were calculated using the ProtScale tool hosted by ExPASy, done for a window size of 3.[53]

peptide (according to the Zimmerman scale)[53] corresponds roughly to a region where the most buried amino acid (according to the "average area buried" scale)[53] is located, with the least buried amino acid placed in close proximity (see Supporting Information Figure S8 and Table S4). It may be possible that the nanoparticle presence provides the buried amino acid's side chain a preferable source of polar interactions compared to the rest of the protein itself, but the data are still insufficient to conclusively support such a model.

A protein's amino acid sequence, electrostatics, and hydrophobicity have been reported to influence the interactions between nanoparticles and the proteins or lipids.[35,58−60] However, few of these studies have attempted to elucidate specific amino acid binding sites on the nanoparticle of interest. One study shows that many of the tryptophanase, alcohol dehydrogenase, bovine serum albumin, and cytochrome *c* peptides found adsorbed to Ag nanoparticles contain at least one histidine residue, and it is proposed that affinity of histidine for metals may be responsible for this adsorption.[61] Another study discussed the potential involvement of basic and polar residues in the binding of poly(acrylic acid)-coated Fe_3O_4 nanoparticles to specific peptides of human serum albumin.[62]

It is possible that only portions of the peptide sequences presented in Table 2 and Supporting Information Figure S6 actually come into contact with the 20S proteasome. If the interactions between the 20S proteasome and 10.5 nm Fe_3O_4 TEGc nanoparticles are due in any part to nonspecific charge interactions, it should be noted that each of the binding "hotspot" sequences except one contains at least one basic amino acid (Table 2 and Supporting Information Figure S6). Calzolai *et al.* identified a patch of electronegative amino acid residues involved in the binding of ubiquitin to Au nanoparticles.[63] In our case, 10.5 nm Fe_3O_4 TEGc nanoparticles appear to primarily contact electrostatically neutral and electronegative patches of the 20S proteasome (Figure 5b and Supporting Information Figure S7). However, many of the binding "hotspots" are adjacent to electropositive regions. The electronegative and electropositive regions of the 20S proteasome are not equally protrusive. In fact, many of the electronegative patches appear to extend away from the protein surface past the electropositive patches. Therefore, it is possible that the negatively charged 10.5 nm Fe_3O_4 TEGc nanoparticles are attracted to the electropositive areas on 20S proteasome complex surface but cannot make a direct contact because of steric reasons. A study by Huhn *et al.* showed that nanoparticle charge had no effect on the number of adsorbed human albumin serum proteins adsorbed to Au nanoparticles,[44] and the peptides identified in this study have a wide range of pI values (3.3−11.5, Table 2). This evidence suggests that electrostatics may not be the only source of adsorption affinity. All but one of the "hotspot" sequences in Table 2 contain at least 25% hydrophilic residues, but overall, minimal colocalization between 10.5 nm Fe_3O_4 and its polar TEGc ligand with the polar residue patches of the 20S proteasome is observed (Figure 5b and Supporting Information Figure S7).

Data in Table 2 list many of the proteasome subunits; most importantly, subunits with enzymatic activity (β1, β2, and β5) bind to the Fe_3O_4 nanoparticles tested. In some cases, more than one amino acid sequence from these proteins binds to nanoparticles, especially at higher nanoparticle concentrations (Tables 2 and Supporting Information Figure S6). Because adsorption of proteins to nanoparticles can deregulate normal protein activity,[32] we anticipated that this may be the case with the 20S proteasome, as well. We investigated proteolytic activity of the 20S proteasome after incubation with different types of nanoparticles for different lengths

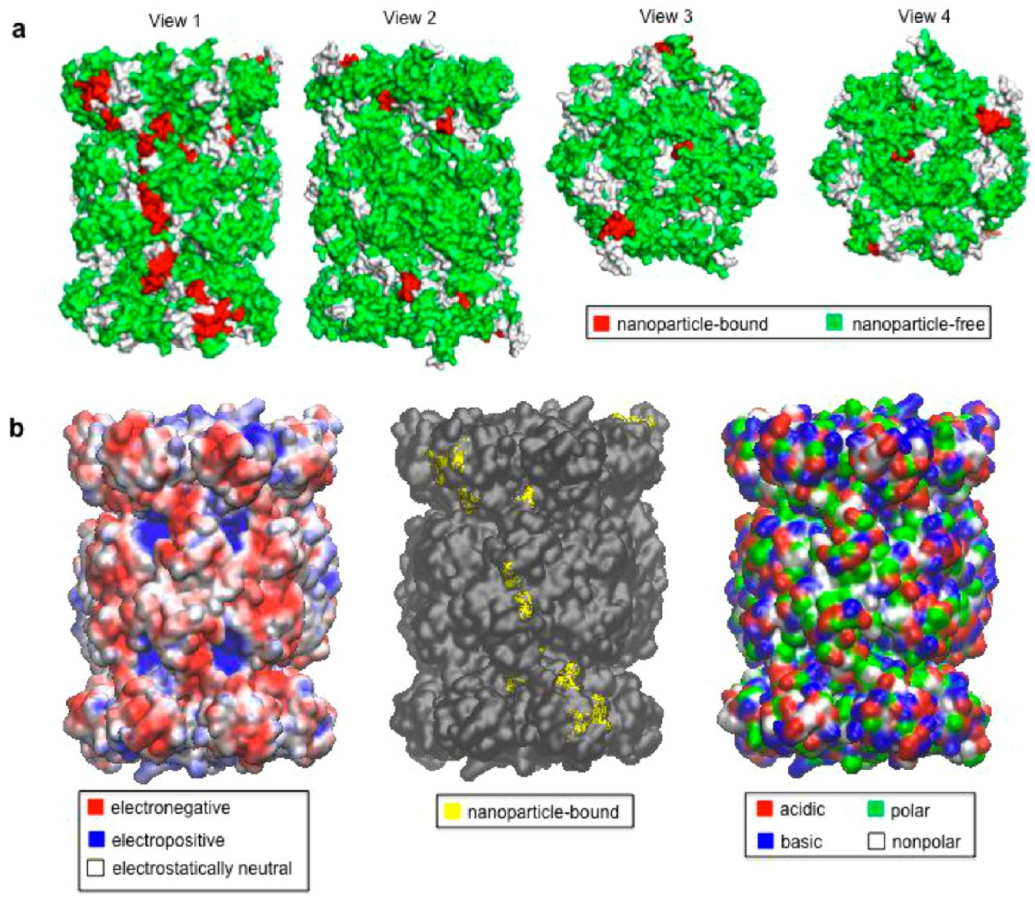

Figure 5. "Hotspots" of adsorption between 10.5 nm Fe_3O_4 TEGc nanoparticles and the 20S proteasome. 440 nM 20S proteasome was incubated with 103.8 nM 10.5 nm Fe_3O_4 TEGc nanoparticles (nanoparticle/protein ratio of 1:4) for 17 h and digested by either trypsin, chymotrypsin, or Asp-N. The nanoparticles were pelleted with the adsorbed peptides, and "free" peptides were analyzed by mass spectrometry. Peptides present in controls but consistently absent following all three digests were considered the peptides most strongly incorporated into the nanoparticle corona. Their sequences are depicted in red in (a) and yellow in (b) and shown in Table 2 and Supporting Information Figure S6. Positions of these peptides, as well as those detected in control and 10.5 nm Fe_3O_4 TEGc nanoparticle-treated samples (green), were located using PyMOL software and the crystal structure of the mammalian 20S proteasome.[52] Together, views 1−4 show the complete 360° surface area of the 20S proteasome. Regions in white in (a) represent peptides not covered by digestion of control or experimental samples, as the enzymes were not 100% proteolytically efficient; it remains to be determined whether these regions contain of nanoparticle binding areas of interest. Additional depleted peptides shorter than 7 amino acids, as well as amino acid sequences missing at higher nanoparticle concentrations, are shown in Supporting Information Figure S6 and Tables S2, S3. (b) View 1 has been expanded to include the electrostatic surface potential and polarity patches of the 20S proteasome using VMD and APBS software and the PDB2PQR web server.[54−57] The remainder of this information for views 2−4 can be found in Supporting Information Figure S7.

of time. Experiments with 5 min, 30 min, 1 h, 1.5 h, 6 h, and 17 h incubation periods were performed. For this study, 1 and 17 h time points were selected as the optimal conditions for illustrating the effects of short-term and long-term interactions between nanoparticles and 20S proteasome. Following incubation of 20S proteasome with nanoparticles, the appropriate aminoluciferin-conjugated peptide substrates, specific for each of the main catalytic activities of the 20S proteasome, were added to reaction mixtures. Peptide−luciferin complexes, LLVY-aminoluciferin, Z-LRR-aminoluciferin, or Z-nLPnLD-aminoluciferin, were used to measure the chymotrypsin-like (β1 subunit-dependent), trypsin-like (β2 subunit-dependent), and caspase-like (β5 subunit-dependent) activities, respectively.

Different concentrations of 10.5 and 4.1 nm Fe_3O_4 TEGc nanoparticles (Figures 6, 7, and Supporting Information Figures S9, S10) modulate the enzymatic activities of the 20S proteasome, especially the trypsin-like (β2 subunit-dependent) activity after incubation for 17 h, more so than any other nanoparticle type studied here. Treatment with 10.5 and 4.1 nm Fe_3O_4 PEG600c nanoparticles also alters enzymatic activities of the 20S proteasome, especially at 17 h, but to a lesser degree. Consistent with the observation that similar total nanoparticle surface areas for TEGc-coated Fe_3O_4 nanoparticles adsorb comparable amounts of the 20S proteasome, higher concentrations of 4.1 nm Fe_3O_4 nanoparticles and lower concentrations of 10.5 nm Fe_3O_4 nanoparticles achieved similar activation of the 20S proteasome (Figures 6, 7, and Supporting Information Figures S9, S10). For example, 0.8 nM 10.5 nm Fe_3O_4 TEGc nanoparticles and 6.3 nM 4.1 nm Fe_3O_4

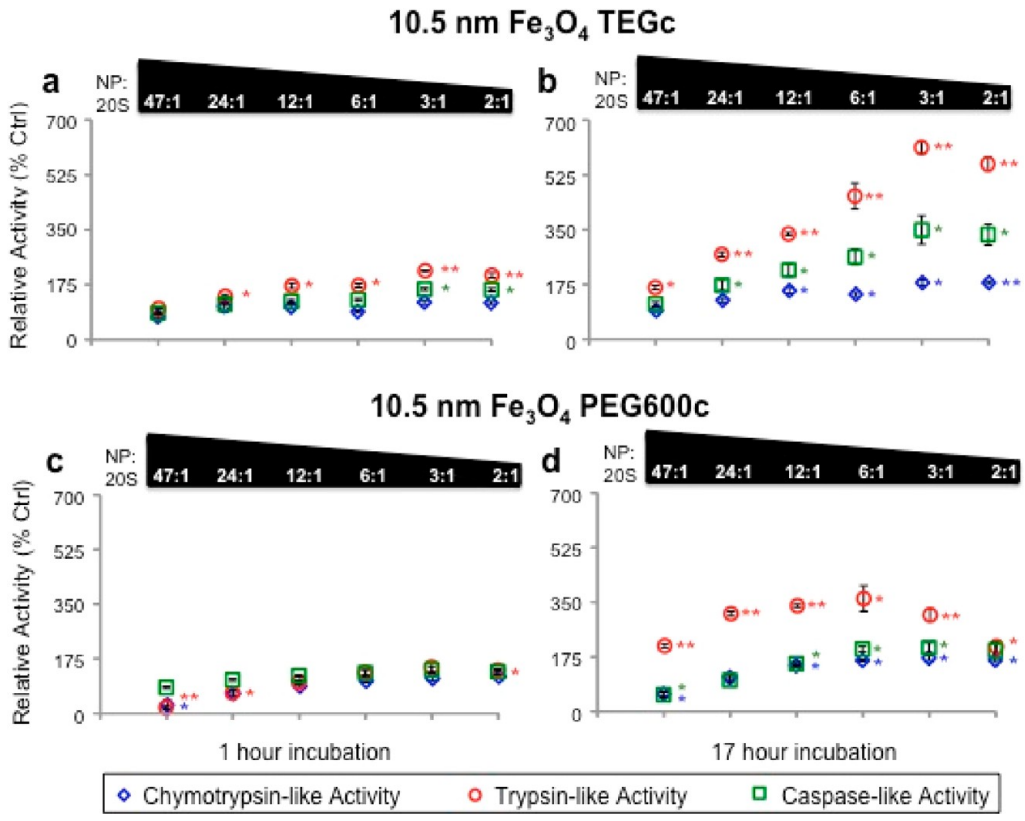

Figure 6. Fluctuations in 20S proteasome activity following incubation with 10.5 nm Fe_3O_4 TEGc and 10.5 nm Fe_3O_4 PEG600c nanoparticles. 20S proteasome (267 pM) was incubated with 10.5, 6.3, 3.1, 1.6, 0.8, or 0.4 nM nanoparticles (left to right) for 1 or 17 h, as shown. Approximate nanoparticle/protein ratios are indicated above the plots as white numbers superimposed on black polygons. Three distinct 20S proteasome activities were evaluated by cleavage-matching luminogenic substrates; each protease activity is indicated separately: chymotrypsin-like activity associated with the β5 subunit (blue diamonds), trypsin-like activity associated with the β2 subunit (red circles), and caspase-like activity associated with the β1 subunit (green squares). Error bars were calculated as standard deviation of two separate experiments, each performed in triplicate. Statistical significance was assessed with an unpaired *t* test, where * reflects a *p* value <0.05 and ** reflects a *p* value <0.01.

TEGc nanoparticles correspond to a total nanoparticle surface area of 1.7×10^{13} and 2.1×10^{13} nm^2, respectively. They each stimulate the trypsin-like activity of 267 pM 20S proteasome by approximately 6.25-fold.

We next decided to compare Fe_3O_4 nanoparticles with the commercially available, "large" superparamagnetic FeraSpin R nanoparticles (Miltenyi Biotec Inc.). None of the FeraSpin R (35 nm) nanoparticle concentrations tested leads to fluctuations in 20S proteasome activity as pronounced as those mediated by 10.5 and 4.1 nm Fe_3O_4 TEGc and PEG600c nanoparticles at any time point (Supporting Information Figure S11).

Finally, we expanded our study to include uncoated TiO_2 nanorods of two sizes and investigated their effects on changes in 20S proteasome activity. In Figure 8 and Supporting Information Figure S12, we show that only the highest concentrations of 20.2 × 3 nm TiO_2 nanorods (nanoparticle/protein ratios in excess of 2:1) stimulate the activity of the 20S proteasome after 17 h. At 1 h, 5.1 × 2.8 nm TiO_2 nanorods more significantly modulate proteasome activity than 20.2 × 3 nm TiO_2 nanorods. At 17 h, 5.1 × 2.8 nm and 20.2 × 3 nm TiO_2 nanorods significantly modulate proteasome activity, but incubation with 5.1 × 2.8 nm TiO_2 nanorods leads to higher activity stimulation than with 20.2 × 3 nm TiO_2 nanorods.

This work suggests that size, charge, surface coating, and shape of nanoparticles may cause dose-dependent changes in 20S proteasome activity. Small nanoparticles may stimulate greater 20S proteasome activity fluctuations than their larger counterparts. For example, at the concentrations tested, the 20S activity fluctuations caused by 10.5 and 4.1 nm Fe_3O_4 TEGc and PEG600c nanoparticles and 5.1 × 2.8 nm TiO_2 nanorods exceed those mediated by FeraSpin R nanoparticles and 20.2 × 3 nm TiO_2 nanorods (Figures 6–8 and Supporting Information Figures S9–S12). Incubation of the 20S proteasome with TEGc-coated nanoparticles may also lead to more profound activity changes than incubation with PEG600c-coated nanoparticles. In addition, nanoparticle charge may play a role in the 20S proteasome activity changes observed, as charge has been shown to significantly impact biologic function.[44,64] In this regard, FeraSpin R nanoparticles, the least negatively charged nanoparticles used in this study, induce the smallest

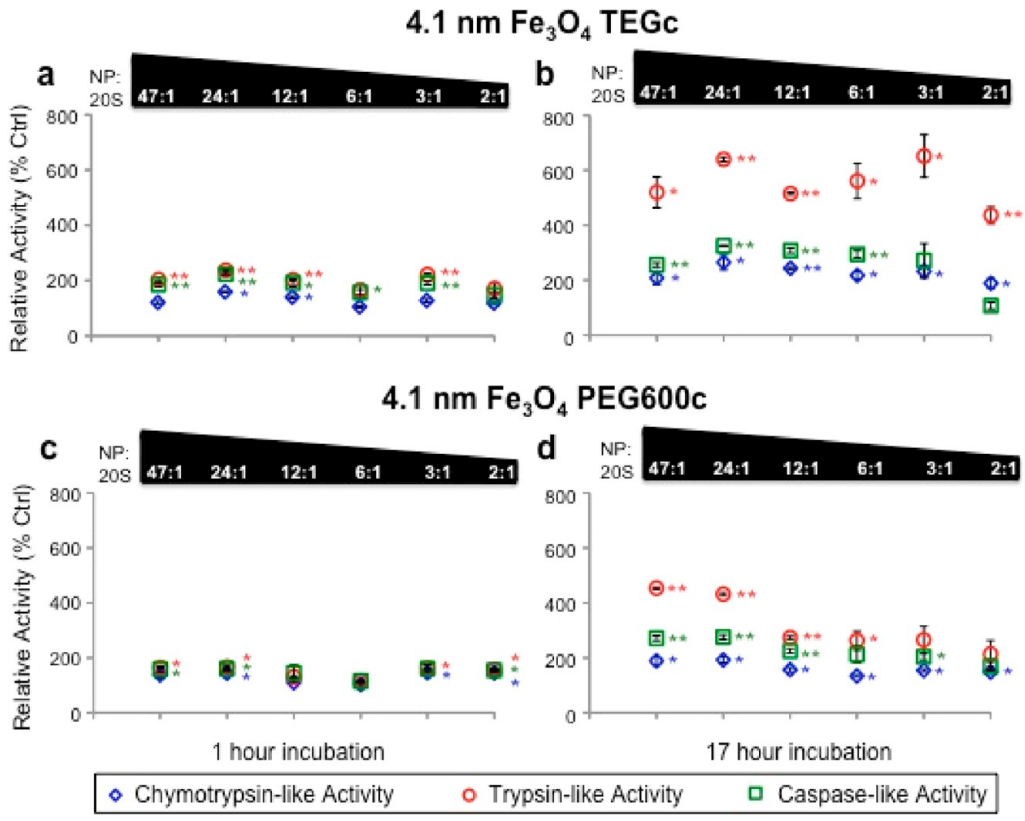

Figure 7. Fluctuations in 20S proteasome activity following incubation with 4.1 nm Fe_3O_4 TEGc and 4.1 nm Fe_3O_4 PEG600c nanoparticles. 20S proteasome (267 pM) was incubated with 10.5, 6.3, 3.1, 1.6, 0.8, or 0.4 nM nanoparticles (left to right) for 1 or 17 h, as shown. Approximate nanoparticle/protein ratios are indicated above the plots as white numbers superimposed on black polygons. Three distinct 20S proteasome activities were evaluated by cleavage-matching luminogenic substrates; each protease activity is indicated separately: chymotrypsin-like activity associated with the β5 subunit (blue diamonds), trypsin-like activity associated with the β2 subunit (red circles), and caspase-like activity associated with the β1 subunit (green squares). Error bars were calculated as standard deviation of two separate experiments, each performed in triplicate. Statistical significance was assessed with an unpaired *t* test, where * reflects a *p* value <0.05 and ** reflects a *p* value <0.01.

activity fluctuations of any of the studied nanoparticles. At the same time, it is well-established that less charged nanoparticles have the greatest potential to form aggregates, which can create other types of complications in *in vivo* uses.[65] An expansion of the collection of nanoparticles used here will be necessary in order to draw more conclusions pertaining to the underlying basis for the effects we have observed. Until more is known about trends in nanoparticle and protein adsorption, every nanoparticle formulation must be carefully studied on a case-by-case basis.

SPR reveals that adsorption of 10.5 and 4.1 nm Fe_3O_4 nanoparticles to 20S proteasome protein occurs rapidly (Supporting Information Figure S4). However, interactions between the 20S proteasome and Fe_3O_4 nanoparticles (or TiO_2 nanorods) for 1 h do not yield the same increase of proteasome activity that was observed after 17 h (Figures 6–8 and Supporting Information Figures S9, S10, and S12). Additional mechanisms, independent of the initial nanoparticle–20S proteasome adsorption event, could also contribute to nanoparticle-mediated changes in 20S proteasome activity. For example, evaluation of 20S proteasome incubated with 10.5 nm Fe_3O_4 TEGc nanoparticles for 1 min, 3 h, or 17 h (Supporting Information Figure S5) by CD suggests that any change in the 20S proteasome complex structure is mild, possibly including a slight modulation in α-helix structures.

Many factors have been shown to alter proteasome activity, including small molecules, post-translational modifications, the association of other proteins, and allosteric effectors such as the 19S proteasome.[66] In the "closed" 20S proteasome conformation, the N-terminal tails of the α subunits lock together and occlude the pore.[12] This leads to low, albeit measurable, levels of proteolysis of peptides and denatured proteins. The binding of the 19S proteasome to the 20S proteasome, however, shifts the N-terminal tails of α subunits, stimulating an "open" conformation ready for elevated substrate translocation and proteolysis.[67,68] The nanoparticles tested here may operate *via* a similar mechanism because a peptide in the N-terminus of the α5 subunit represents a nanoparticle binding "hotspot" identified in this study (Supporting Information Figure S6). The binding of 10.5 nm Fe_3O_4 TEGc nanoparticles to other 20S proteasome subunits which are not involved

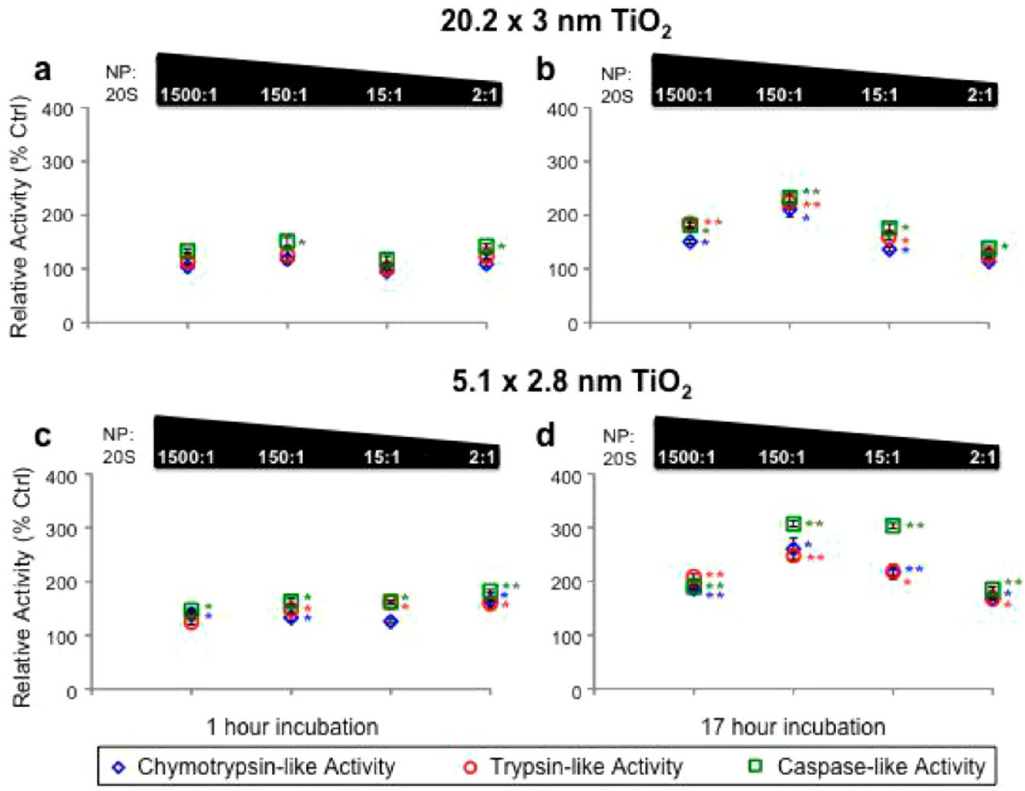

Figure 8. Fluctuations in 20S proteasome activity following incubation with 20.2 × 3 nm and 5.1 × 2.8 nm TiO_2 nanorods. 20S proteasome (267 pM) was incubated with 405, 40.5, 4.5, and 0.45 nM nanorods (left to right) for 1 or 17 h, as shown. Approximate nanoparticle/protein ratios are indicated above the plots as white numbers superimposed on black polygons. Three distinct 20S proteasome activities were evaluated by cleavage-matching luminogenic substrates; each protease activity is indicated separately: chymotrypsin-like activity associated with the β5 subunit (blue diamonds), trypsin-like activity associated with the β2 subunit (red circles), and caspase-like activity associated with the β1 subunit (green squares). Error bars were calculated as standard deviation of two separate experiments, each performed in triplicate. Statistical significance was assessed with an unpaired *t* test, where * reflects a *p* value <0.05 and ** reflects a *p* value <0.01.

in pore formation may also contribute to an open 20S proteasome conformation after a 17 h association period. Because these regions of the α subunits lack secondary structure, any changes in these residues would be undetectable by CD and must be addressed using alternative methods. Alternatively, it is possible that interactions between nanoparticles and the outer surfaces of the β1, β2, and β5 subunits modify their proteolytic behavior, or that adsorption to subunits β6 and β7 alters the inner structure of the proteolytic chamber, increasing the rate of degradation of luminogenic peptides easily entering through the 20S proteasome pore.

Communication between the 19S proteasome and the active sites of the 20S proteasome is documented.[69,70] The 10.5 nm Fe_3O_4 TEGc nanoparticles may show a slight binding preference for the β2 (trypsin-like) subunit over the β1 (caspase-like) and β5 (chymotrypsin-like) subunits (Figure 4), and this could help to explain the differential activity changes observed in this study with 10.5 and 4.1 nm Fe_3O_4 TEGc nanoparticles. While it is necessary to explore these issues further, one of the most important findings of this work remains that 20S proteasome activity, if it is altered by nanoparticle interactions, invariably increases with Fe_3O_4 nanoparticles and TiO_2 nanorods.

We show that 4.1 nm Fe_3O_4 nanoparticles bind to the 20S proteasome and measurably stimulate its activity (Figure 7 and Supporting Information Figure S10). While magnetic resonance imaging applications favor larger nanoparticles,[71] particles of 5 nm in diameter are considered to be less hazardous than their larger counterparts because of the possibility for renal clearance in the whole organism.[72] At this time, it is difficult to predict how the effects of metal oxide nanoparticles on 20S proteasome binding and activity will translate to an *in vivo* situation. If metal oxide nanoparticles modulate 20S proteasome activity in cells *in vivo* as they do in experimental conditions used here, cellular homeostasis could be compromised. Several aspects of metal oxide nanoparticle-induced cytotoxicity studies suggest possible changes in proteasome-regulated processes.[73−75] It is plausible that endosomal escape of nanoparticles could lead to direct interaction with the proteasome, and it is likely that the cellular damage caused by agents that deregulate all three proteasome activities would be significant. Bortezomib, a small-molecule proteasome inhibitor

approved by the FDA for the treatment of multiple myeloma and mantle cell lymphoma, was found to be less cytotoxic than originally anticipated because it inhibits primarily the chymotrypsin-like activity of the 20S proteasome.[76] In effect, nanoparticles that relatively equally alter the chymotrypsin-, trypsin-, and caspase-like activities of the 20S proteasome, such as 20.2 × 3 nm and 5.1 × 2.8 nm TiO_2 nanorods, could pose greater risks than those that preferentially modulate one catalytic activity and do not affect the others, such as 10.5 and 4.1 nm Fe_3O_4 nanoparticles.

CONCLUSIONS

Until now, nanoparticle adsorption to the proteasome has rarely been studied, and to the best of our knowledge, nanoparticles have not previously been tested as modulators of proteasome activity. In this study, we have found that several metal oxide nanoparticles bind to the 20S proteasome with varying capabilities; 10.5 nm Fe_3O_4 TEGc nanoparticles and others may have a preference for specific 20S proteasome subunits. Interaction between metal oxide nanoparticles and the 20S proteasome can result in induction of proteasome activity *in vitro*, and the different properties of these nanoparticles have different effects on 20S proteasome activity fluctuations. Because the proteasome is abundant in cells and regulates the majority of cellular processes, nanoparticle-induced interference with cellular proteasome activity may pose a cytotoxicity concern. Conversely, in those diseases where decrease of proteasome activity is noted, nanoparticle enhancers of proteasome activity may open new avenues for treatment.

METHODS

Nanoparticle Preparation. Fe_3O_4 nanoparticles were prepared according to a reported procedure.[77] Following synthesis, the nanoparticle mixture was diluted 20:1 with a 1:1 mixture of ethyl acetate and methanol. Nanoparticles were separated by magnet overnight, and the procedure was repeated five times. The final purified particles were dispersed in hexane. To transfer the Fe_3O_4 nanoparticles from hexane to water, a ligand composed of a nitrodopamine and a carboxylate-terminated polyethyleneglycol was used. All chemicals were purchased from Sigma.

TiO_2 nanorods were synthesized *via* a high-temperature nonhydrolytic method developed previously.[48] TiO_2 nanorods (10 mg) were dispersed in 4 mL of 1 M tetramethylammonium hydroxide in butanol. The reaction mixture was incubated for 1 h with sonication, and the TiO_2 nanorods were collected by centrifugation and redispersed in nanopure water.[49] All chemicals were purchased from Sigma.

Nanoparticle Characterization. Nanoparticle sizes were quantified by transmission electron microscopy (TEM). Dynamic light scattering (DLS) and zeta-potential measurements were taken using a Malvern Zetasizer Nano instrument. Nanoparticles were dispersed in nanopure H_2O, and a minimum of three measurements per sample was made at 25 °C. Nanoparticle molarity was calculated based on [Fe] and [Ti] concentrations obtained by inductively coupled plasma atomic emission spectroscopy (ICP-AES) of acid digested samples, taking into account nanoparticle size obtained by TEM, Fe_3O_4 density (5.17 g/cm^3) or anatase TiO_2 density (3.88 g/cm^3), and Avogadro's number.

Western Blot for Nanoparticle–20S Proteasome Binding. Two micrograms of purified 20S proteasome protein (R&D Systems) in 10 mM HEPES (Sigma, pH 7.6) was incubated with or without nanoparticles at 25 °C for 17 h. All samples were centrifuged (13 000 rcf, 15 min) in the presence of 4.5 M NaCl (Sigma). All supernatants were desalted using Zeba spin desalting columns (Thermo Scientific) and dried *in vacuo*. The protein was resolubilized, resolved *via* SDS-PAGE, and transferred to an Immobilon-P PVDR membrane (Thermo Scientific). Membrane was blocked overnight with 5% nonfat dry milk and probed for 1 h with a monoclonal antibody for the 20S proteasome α2 subunit (Enzo Life Sciences). Following incubation with a horseradish peroxidase-conjugated secondary antibody (Cell Signaling Technology), membrane was visualized with the Pierce SuperSignal chemiluminescent substrate (Thermo Scientific).

Trypsin Digestion for 20S Proteasome Quantity. Two micrograms of purified 20S proteasome protein in 10 mM HEPES (Sigma, pH 7.6) was incubated with or without 10.5 nm Fe_3O_4 TEGc nanoparticles at 25 °C for 17 h. All samples were centrifuged (13 000 rcf, 15 min) in the presence of 4.5 M NaCl (Sigma). All supernatants were desalted using Zeba spin desalting columns (Thermo Scientific) and dried *in vacuo*. Protein was resolubilized in 8 M urea (Sigma), dissolved in 40 mM ammonium bicarbonate (Sigma), and denatured (60 °C, 45 min). Protein was reduced with 2.4 mM dithiothreitol (Sigma, 60 °C, 15 min) and alkylated in the dark with 4.5 mM iodoacetamide (Sigma) (25 °C, 15 min). Protein was digested with 200 ng of sequencing grade trypsin (Sigma) overnight at 37 °C, and the resulting peptides were identified by mass spectrometry.

Digestion for Nanoparticle–20S Proteasome Adsorption Specificity. Two micrograms of purified 20S proteasome protein in HEPES (Sigma, pH 7.6) was incubated with or without 10.5 nm Fe_3O_4 TEGc nanoparticles at 25 °C for 17 h. All samples were dried *in vacuo* and resolubilized in 8 M urea (Sigma), dissolved in 40 mM ammonium bicarbonate (Sigma). The protein was denatured (60 °C, 45 min), reduced with 2.4 mM dithiothreitol (Sigma, 60 °C, 15 min), and alkylated in the dark with 4.5 mM iodoacetamide (Sigma, 25 °C, 15 min). Protein was digested with 200 ng of sequencing grade trypsin (Sigma) at 37 °C, 100 ng of chymotrypsin (Promega) at 25 °C, or 100 ng of Asp-N (Promega) at 37 °C for 18 h. Following digestion, all samples were centrifuged (13 000 rcf, 15 min) in the presence of 4.5 M NaCl, and the peptides remaining in the supernatant were identified by mass spectrometry (see below).

Peptide Identification by Mass Spectrometry. The digested protein preparation was first dried *in vacuo* and resuspended in 500 μL of 5% acetonitrile and 0.1% formic acid (Sigma). The samples were further desalted using C18 spin columns (Thermoscientific). The desalted peptides were loaded directly onto a 10 cm long, 75 μM reversed-phase capillary column (ProteoPep II C18, 300 Å, 5 μm size, New Objective) and separated with a 100 min gradient from 5% acetonitrile to 100% acetonitrile on a Proxeon Easy n-LC II (Thermo Scientific). The peptides were directly eluted into an LTQ Orbitrap Velos mass spectrometer (Thermo Scientific) with electrospray ionization at 350 nL/min flow rate. The mass spectrometer was operated in data-dependent mode, and for each MS1 precursor ion scan, the 10 most intense ions were selected from fragmentation by CID (collision-induced dissociation). The other parameters for mass spectrometry analysis were as follows: resolution of MS1 was set at 60 000, normalized collision energy 35%, activation time 10 ms, isolation width 1.5, and the +1 and +4 and higher charge states were rejected.

The data were processed using Proteome Discoverer (version 1.3, Thermo Scientific) and searched using an in-house MASCOT server. The data were searched against the Swiss-Prot database (version 2011_12). The species filters for database search for samples was *Homo sapiens*. The other parameters were as follows: (i) enzyme specificity, trypsin; (ii) fixed modification, cysteine carbamidomethylation; (iv) variable modification, methionine oxidation and N-terminal acetylation; (v) precursor mass tolerance was ±10 ppm; and (vi) fragment ion

mass tolerance was ±0.8 Da. All the spectra were searched against target/decoy databases, and the mascot significance threshold was chosen to achieve a targeted false discovery rate of 1%. The peptide identification was considered valid if its corresponding mascot score was equal to or less than the threshold. Protein grouping was enabled in Proteome Discoverer, and proteins were grouped to satisfy the rule of parsimony.

Mass Spectrometry Quantification and Analysis. Spectral counting was used as a measure of differential quantification between control and nanoparticle-treated purified 20S proteasome. The total number of peptide spectral matches (PSMs) corresponding to a particular 20S proteasome subunit was calculated for each sample as described above. The % relative quantitative differences correspond to the ratios of total spectral counts assigned for each subunit in control and nanoparticle-treated samples. Results and standard error shown are representative of the means of three control and three experimental samples.

Coverage of each 20S proteasome subunit was calculated for each sample as a measure of the full sequence of each protein identified by mass spectrometry. Coverage of each subunit of the experimental (nanoparticle-treated) samples was compared to the coverage of each corresponding subunit of the control samples. Results and standard error shown are representative of the means of three control and three experimental samples.

The isoelectric point (pI) of each peptide implicated in nanoparticle binding was calculated according to the Lehninger scale. The net charges at pH 7.6 and 8.0 were calculated using the Peptide Property Calculator (Innovagen). Peptide hydrophobicity, polarity, hydropathicity, and "average area buried on transfer from standard state to folded protein" were calculated using ProtScale tool online at the Web site http://web.expasy.org/protscale.[53] Only polarity according to Zimmerman and the "average area buried" values (Supporting Information Table S4) are presented in the Table 2 and Supporting Information Figure S8, as they suggest a combined peptide content pattern.

Visualization of Nanoparticle Binding Hotspots and 20S Proteasome Electrostatics. The crystal structure of the mammalian 20S proteasome (PDB ID: 1IRU) was opened with MacPyMOL (version 1.3), and the surface representation option was chosen. The amino acid sequences implicated in the adsorption of nanoparticles to the 20S proteasome, as determined by mass spectrometry, were selected using the color tool.

To visualize the electrostatics of the 20S proteasome (PDB ID: 1IRU), the PDB2PQR web server was first employed selecting the PARSE forcefield and internal naming scheme options.[54,55] The generated PQR file was loaded into VMD software.[57] The electrostatics calculations were performed using the Adaptive Poisson−Boltzmann Solver (APBS, version 1.4) tool.[56] From the Graphical Representations window, the "Quick Surf" Drawing Method and "Volume" Coloring Method were selected, and the Color Scale Data Range was set to −3 to 3. Separately, the polarity patches of the 20S proteasome were displayed using the "Quick Surf" Drawing Method and "ResType" Coloring Method in VMD.

20S Proteasome Activity Measurements. Twenty or 100 ng of 20S proteasome protein in 10 mM HEPES (pH 7.6, Sigma) was incubated with nanoparticles in white 96-well microplates (Enzo Life Sciences) in the dark at 25 °C for 1 or 17 h. Luciferin detection reagent supplemented with (i) 40 μM Suc-LLVY-aminoluciferin, (ii) 30 μM Z-LRR-aminoluciferin, or (iii) Z-nLPnLD-aminoluciferin (Promega Corporation) was then added to the samples to measure the chymotrypsin-, trypsin-, and caspase-like 20S proteasome activities, respectively. Luminescence was detected using a SpectraMax M5 plate reader 10 min after luciferin detection reagent addition. To reflect solely nanoparticle-induced alterations of 20S proteasome activity, background luminescence and the effects of nanoparticles on luminescence/luciferase activity were taken into consideration in the interpretation of data. Briefly, nanoparticles were incubated with luciferin detection reagent supplemented with D-aminoluciferin (Assay Biotech). The resulting luminescence was measured, and nanoparticle-stimulated changes in luminescence were subtracted from the 20S proteasome activity measurements taken in the presence of nanoparticles.

Conflict of Interest: The authors declare no competing financial interest.

Acknowledgment. C.A.F., T.P., and G.E.W. are supported by the NIH/NCI T32CA09560, NIH/NIBIB R01EB002100, and NIH/NCI U54 CA151880 grants. J.K. and J.S. are supported by grants from the Kentucky Science and Engineering Foundation (KSEF-148-502-06-189) and the Kentucky Tobacco Research and Development Center (Lexington, KY, USA). S.S.C., M.D., and V.P.D. are funded by the National Cancer Institute Center for Cancer Nanotechnology Excellence (CCNE) initiative at Northwestern University, Award No. U54CA119341. A.W. is supported by the Natural Science Foundation of China (31128007 and 31170964), the Hundred Talents Program (2010-735), and the Strategic Leading Science and Technology Projects of Chinese Academy of Sciences. J.C. is supported by the National Creative Research Initiatives Program (2010-0018286). This work used resources of the Proteomics Core, which is funded by the Office of Research of Northwestern University, and the Keck Biophysics Facility, which is supported in part by the NCI CCSG P30 CA060553 grant awarded to the Robert H Lurie Comprehensive Cancer Center. The authors would like to thank A. Grigorescu, C. Janczak, and M. Dennis from the Keck Biophysics Facility of Northwestern University for their constant assistance and support.

Supporting Information Available: Figure S1. TEM images of nanoparticles used in this work. Figure S2. TEM images of 10.5 nm Fe_3O_4 TEGc nanoparticles co-incubated with the 20S proteasome. Figure S3. Western blot showing behavior of 20S proteasome complex at high ionic strength conditions in the presence or absence of 10.5 nm Fe_3O_4 TEGc nanoparticles. Figure S4. Surface plasmon resonance sensorgrams. Figure S5. Circular dichroism spectra of 20S proteasome with 10.5 nm Fe_3O_4 TEGc nanoparticles. Figure S6. Full 20S proteasome subunit sequences indicating peptides involved in the adsorption of the 20S proteasome to 10.5 nm Fe_3O_4 TEGc nanoparticles. Figure S7. Additional electrostatic and polarity representations of the 20S proteasome (continuation of Figure 5b). Figure S8. Local Zimmerman polarity and "average area buried on transfer from standard state to folded protein" calculations for peptides from Table 2. Figures S9, S10, and S12. Proteolytic activity curves for 100 ng 20S proteasome with 10.5 and 4.1 nm Fe_3O_4 nanoparticles and 20.2 × 3 and 5.1 × 2.8 nm TiO_2 nanorods. Figure S11. Proteolytic activity curves with FeraSpin R nanoparticles. Table S1. Additional zeta-potential measurements of nanoparticles used in this work. Tables S2 and S3. Additional mass spectrometry data with 10.5 and 4.1 nm Fe_3O_4 nanoparticles. Table S4. Scales used for calculations in Figure S8. This material is available free of charge *via* the Internet at http://pubs.acs.org.

REFERENCES AND NOTES

1. Glickman, M. H.; Ciechanover, A. The Ubiquitin−Proteasome Proteolytic Pathway: Destruction for the Sake of Construction. *Physiol. Rev.* **2002**, *82*, 373–428.
2. Finley, D. Recognition and Processing of Ubiquitin−Protein Conjugates by the Proteasome. *Annu. Rev. Biochem.* **2009**, *78*, 477–513.
3. Voges, D.; Zwickl, P.; Baumeister, W. The 26S Proteasome: A Molecular Machine Designed for Controlled Proteolysis. *Annu. Rev. Biochem.* **1999**, *68*, 1015–1068.
4. Navon, A.; Ciechanover, A. The 26 S Proteasome: From Basic Mechanisms to Drug Targeting. *J. Biol. Chem.* **2009**, *284*, 33713–33718.
5. Scheffner, M.; Nuber, U.; Huibregtse, J. M. Protein Ubiquitination Involving an E1-E2-E3 Enzyme Ubiquitin Thioester Cascade. *Nature* **1995**, *373*, 81–83.
6. Bech-Otschir, D.; Helfrich, A.; Enenkel, C.; Consiglieri, G.; Seeger, M.; Holzhutter, H. G.; Dahlmann, B.; Kloetzel, P. M. Polyubiquitin Substrates Allosterically Activate Their Own Degradation by the 26S Proteasome. *Nat. Struct. Mol. Biol.* **2009**, *16*, 219–225.
7. Nickell, S.; Beck, F.; Scheres, S. H.; Korinek, A.; Forster, F.; Lasker, K.; Mihalache, O.; Sun, N.; Nagy, I.; Sali, A.; *et al.* Insights into the Molecular Architecture of the 26S Proteasome. *Proc. Natl. Acad. Sci. U.S.A.* **2009**, *106*, 11943–11947.
8. da Fonseca, P. C.; Morris, E. P. Structure of the Human 26S Proteasome: Subunit Radial Displacements Open the Gate into the Proteolytic Core. *J. Biol. Chem.* **2008**, *283*, 23305–23314.

9. Groll, M.; Ditzel, L.; Lowe, J.; Stock, D.; Bochtler, M.; Bartunik, H. D.; Huber, R. Structure of 20S Proteasome from Yeast at 2.4 Å Resolution. *Nature* **1997**, *386*, 463–471.
10. Orlowski, M.; Wilk, S. Catalytic Activities of the 20 S Proteasome, a Multicatalytic Proteinase Complex. *Arch. Biochem. Biophys.* **2000**, *383*, 1–16.
11. Chu-Ping, M.; Vu, J. H.; Proske, R. J.; Slaughter, C. A.; DeMartino, G. N. Identification, Purification, and Characterization of a High Molecular Weight, ATP-Dependent Activator (Pa700) of the 20 S Proteasome. *J. Biol. Chem.* **1994**, *269*, 3539–3547.
12. Groll, M.; Bajorek, M.; Kohler, A.; Moroder, L.; Rubin, D. M.; Huber, R.; Glickman, M. H.; Finley, D. A Gated Channel into the Proteasome Core Particle. *Nat. Struct. Biol.* **2000**, *7*, 1062–1067.
13. Liu, C. W.; Jacobson, A. D. Functions of the 19S Complex in Proteasomal Degradation. *Trends Biochem. Sci.* **2013**, *38*, 103–110.
14. Rosenzweig, R.; Osmulski, P. A.; Gaczynska, M.; Glickman, M. H. The Central Unit within the 19S Regulatory Particle of the Proteasome. *Nat. Struct. Mol. Biol.* **2008**, *15*, 573–580.
15. Schwartz, A. L.; Ciechanover, A. The Ubiquitin–Proteasome Pathway and Pathogenesis of Human Diseases. *Annu. Rev. Med.* **1999**, *50*, 57–74.
16. Schwartz, A. L.; Ciechanover, A. Targeting Proteins for Destruction by the Ubiquitin System: Implications for Human Pathobiology. *Annu. Rev. Pharmacol. Toxicol.* **2009**, *49*, 73–96.
17. Bulteau, A. L.; Lundberg, K. C.; Humphries, K. M.; Sadek, H. A.; Szweda, P. A.; Friguet, B.; Szweda, L. I. Oxidative Modification and Inactivation of the Proteasome during Coronary Occlusion/Reperfusion. *J. Biol. Chem.* **2001**, *276*, 30057–30063.
18. Dahlmann, B. Role of Proteasomes in Disease. *BMC Biochem.* **2007**, *8*, S3.
19. Seeger, M.; Ferrell, K.; Frank, R.; Dubiel, W. Hiv-1 Tat Inhibits the 20 S Proteasome and Its 11 S Regulator-Mediated Activation. *J. Biol. Chem.* **1997**, *272*, 8145–8148.
20. Zhao, X.; Yang, J. Amyloid-Beta Peptide Is a Substrate of the Human 20S Proteasome. *ACS Chem. Neurosci.* **2010**, *1*, 655–660.
21. McNaught, K. S.; Jenner, P. Proteasomal Function Is Impaired in Substantia Nigra in Parkinson's Disease. *Neurosci. Lett.* **2001**, *297*, 191–194.
22. Keller, J. N.; Hanni, K. B.; Markesbery, W. R. Impaired Proteasome Function in Alzheimer's Disease. *J. Neurochem.* **2000**, *75*, 436–439.
23. Frankland-Searby, S.; Bhaumik, S. R. The 26S Proteasome Complex: An Attractive Target for Cancer Therapy. *Biochim. Biophys. Acta* **2012**, *1825*, 64–76.
24. Chen, L.; Madura, K. Increased Proteasome Activity, Ubiquitin-Conjugating Enzymes, and Eef1a Translation Factor Detected in Breast Cancer Tissue. *Cancer Res.* **2005**, *65*, 5599–5606.
25. Edwards, C. M.; Lwin, S. T.; Fowler, J. A.; Oyajobi, B. O.; Zhuang, J.; Bates, A. L.; Mundy, G. R. Myeloma Cells Exhibit an Increase in Proteasome Activity and an Enhanced Response to Proteasome Inhibition in the Bone Marrow Microenvironment *in Vivo*. *Am. J. Hematol.* **2009**, *84*, 268–272.
26. Unfried, K.; Albrecht, C.; Klotz, L.; Von Mikecz, A.; Grether-Beck, S.; Schins, R. P. Cellular Responses to Nanoparticles: Target Structures and Mechanisms. *Nanotoxicology* **2007**, *1*, 52–71.
27. Dutta, D.; Sundaram, S. K.; Teeguarden, J. G.; Riley, B. J.; Fifield, L. S.; Jacobs, J. M.; Addleman, S. R.; Kaysen, G. A.; Moudgil, B. M.; Weber, T. J. Adsorbed Proteins Influence the Biological Activity and Molecular Targeting of Nanomaterials. *Toxicol. Sci.* **2007**, *100*, 303–315.
28. Lesniak, A.; Fenaroli, F.; Monopoli, M. P.; Aberg, C.; Dawson, K. A.; Salvati, A. Effects of the Presence or Absence of a Protein Corona on Silica Nanoparticle Uptake and Impact on Cells. *ACS Nano* **2012**, *6*, 5845–5857.
29. Monopoli, M. P.; Aberg, C.; Salvati, A.; Dawson, K. A. Biomolecular Coronas Provide the Biological Identity of Nanosized Materials. *Nat. Nanotechnol.* **2012**, *7*, 779–786.
30. Salvati, A.; Pitek, A. S.; Monopoli, M. P.; Prapainop, K.; Bombelli, F. B.; Hristov, D. R.; Kelly, P. M.; Aberg, C.; Mahon, E.; Dawson, K. A. Transferrin-Functionalized Nanoparticles Lose Their Targeting Capabilities When a Biomolecule Corona Adsorbs on the Surface. *Nat. Nanotechnol.* **2013**, *8*, 137–143.
31. Deng, Z. J.; Liang, M.; Monteiro, M.; Toth, I.; Minchin, R. F. Nanoparticle-Induced Unfolding of Fibrinogen Promotes Mac-1 Receptor Activation and Inflammation. *Nat. Nanotechnol.* **2011**, *6*, 39–44.
32. Wu, Z.; Zhang, B.; Yan, B. Regulation of Enzyme Activity through Interactions with Nanoparticles. *Int. J. Mol. Sci.* **2009**, *10*, 4198–4209.
33. Sousa, S. R.; Moradas-Ferreira, P.; Saramago, B.; Melo, L. V.; Barbosa, M. A. Human Serum Albumin Adsorption on TiO_2 from Single Protein Solutions and from Plasma. *Langmuir* **2004**, *20*, 9745–9754.
34. Cedervall, T.; Lynch, I.; Foy, M.; Berggard, T.; Donnelly, S. C.; Cagney, G.; Linse, S.; Dawson, K. A. Detailed Identification of Plasma Proteins Adsorbed on Copolymer Nanoparticles. *Angew. Chem., Int. Ed.* **2007**, *46*, 5754–5756.
35. Cedervall, T.; Lynch, I.; Lindman, S.; Berggard, T.; Thulin, E.; Nilsson, H.; Dawson, K. A.; Linse, S. Understanding the Nanoparticle–Protein Corona Using Methods To Quantify Exchange Rates and Affinities of Proteins for Nanoparticles. *Proc. Natl. Acad. Sci. U.S.A.* **2007**, *104*, 2050–2055.
36. Lundqvist, M.; Stigler, J.; Elia, G.; Lynch, I.; Cedervall, T.; Dawson, K. A. Nanoparticle Size and Surface Properties Determine the Protein Corona with Possible Implications for Biological Impacts. *Proc. Natl. Acad. Sci. U.S.A.* **2008**, *105*, 14265–14270.
37. Havugimana, P. C.; Hart, G. T.; Nepusz, T.; Yang, H.; Turinsky, A. L.; Li, Z.; Wang, P. I.; Boutz, D. R.; Fong, V.; Phanse, S.; *et al.* A Census of Human Soluble Protein Complexes. *Cell* **2012**, *150*, 1068–1081.
38. Hoffmann, O.; Heubner, M.; Anlasik, T.; Winterhalter, M.; Dahlmann, B.; Kasimir-Bauer, S.; Kimmig, R.; Wohlschlaeger, J.; Sixt, S. U. Circulating 20S Proteasome in Patients with Non-metastasized Breast Cancer. *Anticancer Res.* **2011**, *31*, 2197–2201.
39. Lundqvist, M.; Stigler, J.; Cedervall, T.; Berggard, T.; Flanagan, M. B.; Lynch, I.; Elia, G.; Dawson, K. The Evolution of the Protein Corona around Nanoparticles: A Test Study. *ACS Nano* **2011**, *5*, 7503–7509.
40. Huang, R.; Carney, R. P.; Stellacci, F.; Lau, B. L. Protein–Nanoparticle Interactions: The Effects of Surface Compositional and Structural Heterogeneity Are Scale Dependent. *Nanoscale* **2013**, *5*, 6928–6935.
41. Schaffler, M.; Semmler-Behnke, M.; Sarioglu, H.; Takenaka, S.; Wenk, A.; Schleh, C.; Hauck, S. M.; Johnston, B. D.; Kreyling, W. G. Serum Protein Identification and Quantification of the Corona of 5, 15 and 80 nm Gold Nanoparticles. *Nanotechnology* **2013**, *24*, 265103.
42. Yang, J. A.; Johnson, B. J.; Wu, S.; Woods, W. S.; George, J. M.; Murphy, C. J. Study of Wild-Type Alpha-Synuclein Binding and Orientation on Gold Nanoparticles. *Langmuir* **2013**, *29*, 4603–4615.
43. Ashby, J.; Schachermeyer, S.; Pan, S.; Zhong, W. Dissociation-Based Screening of Nanoparticle–Protein Interaction *via* Flow Field-Flow Fractionation. *Anal. Chem.* **2013**, *85*, 7494–7501.
44. Huhn, D.; Kantner, K.; Geidel, C.; Brandholt, S.; De Cock, I.; Soenen, S. J.; Rivera Gil, P.; Montenegro, J. M.; Braeckmans, K.; Mullen, K.; *et al.* Polymer-Coated Nanoparticles Interacting with Proteins and Cells: Focusing on the Sign of the Net Charge. *ACS Nano* **2013**, *7*, 3253–3263.
45. O'Brien, E. P.; Straub, J. E.; Brooks, B. R.; Thirumalai, D. Influence of Nanoparticle Size and Shape on Oligomer Formation of an Amyloidogenic Peptide. *J. Phys. Chem. Lett.* **2011**, *2*, 1171–1177.
46. Aggarwal, P.; Hall, J. B.; McLeland, C. B.; Dobrovolskaia, M. A.; McNeil, S. E. Nanoparticle Interaction with Plasma Proteins as It Relates to Particle Biodistribution, Biocompatibility and Therapeutic Efficacy. *Adv. Drug Delivery Rev.* **2009**, *61*, 428–437.

47. Prosen, L.; Prijic, S.; Music, B.; Lavrencak, J.; Cemazar, M.; Sersa, G. Magnetofection: A Reproducible Method for Gene Delivery to Melanoma Cells. *Biomed. Res. Int.* **2013**, *2013*, 209452.
48. Seo, J. W.; Chung, H.; Kim, M. Y.; Lee, J.; Choi, I. H.; Cheon, J. Development of Water-Soluble Single-Crystalline TiO_2 Nanoparticles for Photocatalytic Cancer-Cell Treatment. *Small* **2007**, *3*, 850–853.
49. Salgueirino-Maceira, V.; Liz-Marzan, L. M.; Farle, M. Water-Based Ferrofluids from Fexpt1-X Nanoparticles Synthesized in Organic Media. *Langmuir* **2004**, *20*, 6946–6950.
50. Johnson, W. C., Jr. Protein Secondary Structure and Circular Dichroism: A Practical Guide. *Proteins* **1990**, *7*, 205–214.
51. Olsen, J. V.; Ong, S. E.; Mann, M. Trypsin Cleaves Exclusively C-Terminal to Arginine and Lysine Residues. *Mol. Cell. Proteomics* **2004**, *3*, 608–614.
52. Unno, M.; Mizushima, T.; Morimoto, Y.; Tomisugi, Y.; Tanaka, K.; Yasuoka, N.; Tsukihara, T. The Structure of the Mammalian 20S Proteasome at 2.75 Å Resolution. *Structure* **2002**, *10*, 609–618.
53. Wilkins, M. R.; Gasteiger, E.; Bairoch, A.; Sanchez, J. C.; Williams, K. L.; Appel, R. D.; Hochstrasser, D. F. Protein Identification and Analysis Tools in the Expasy Server. *Methods Mol. Biol.* **1999**, *112*, 531–552.
54. Dolinsky, T. J.; Czodrowski, P.; Li, H.; Nielsen, J. E.; Jensen, J. H.; Klebe, G.; Baker, N. A. Pdb2pqr: Expanding and Upgrading Automated Preparation of Biomolecular Structures for Molecular Simulations. *Nucleic Acids Res.* **2007**, *35*, W522–525.
55. Dolinsky, T. J.; Nielsen, J. E.; McCammon, J. A.; Baker, N. A. Pdb2pqr: An Automated Pipeline for the Setup of Poisson–Boltzmann Electrostatics Calculations. *Nucleic Acids Res.* **2004**, *32*, W665–667.
56. Baker, N. A.; Sept, D.; Joseph, S.; Holst, M. J.; McCammon, J. A. Electrostatics of Nanosystems: Application to Microtubules and the Ribosome. *Proc. Natl. Acad. Sci. U.S.A.* **2001**, *98*, 10037–10041.
57. Humphrey, W.; Dalke, A.; Schulten, K. VMD: Visual Molecular Dynamics. *J. Mol. Graphics* **1996**, *14*, 27–38.
58. Chang, S. Y.; Zheng, N. Y.; Chen, C. S.; Chen, C. D.; Chen, Y. Y.; Wang, C. R. Analysis of Peptides and Proteins Affinity-Bound to Iron Oxide Nanoparticles by MALDI MS. *J. Am. Soc. Mass Spectrom.* **2007**, *18*, 910–918.
59. Xiao, X.; Montano, G. A.; Edwards, T. L.; Allen, A.; Achyuthan, K. E.; Polsky, R.; Wheeler, D. R.; Brozik, S. M. Surface Charge Dependent Nanoparticle Disruption and Deposition of Lipid Bilayer Assemblies. *Langmuir* **2012**, *28*, 17396–17403.
60. Lynch, I.; Dawson, K. A.; Linse, S. Detecting Cryptic Epitopes Created by Nanoparticles. *Sci. STKE* **2006**, *327*, pe14.
61. Wigginton, N. S.; de Titta, A.; Piccapietra, F.; Dobias, J.; Nesatyy, V. J.; Suter, M. J.; Bernier-Latmani, R. Binding of Silver Nanoparticles to Bacterial Proteins Depends on Surface Modifications and Inhibits Enzymatic Activity. *Environ. Sci. Technol.* **2010**, *44*, 2163–2168.
62. Li, N.; Zeng, S.; He, L.; Zhong, W. Exploration of Possible Binding Sites of Nanoparticles on Protein by Cross-Linking Chemistry Coupled with Mass Spectrometry. *Anal. Chem.* **2011**, *83*, 6929–6934.
63. Calzolai, L.; Franchini, F.; Gilliland, D.; Rossi, F. Protein–Nanoparticle Interaction: Identification of the Ubiquitin–Gold Nanoparticle Interaction Site. *Nano Lett.* **2010**, *10*, 3101–3105.
64. Schaeublin, N. M.; Braydich-Stolle, L. K.; Schrand, A. M.; Miller, J. M.; Hutchison, J.; Schlager, J. J.; Hussain, S. M. Surface Charge of Gold Nanoparticles Mediates Mechanism of Toxicity. *Nanoscale* **2011**, *3*, 410–420.
65. Bagwe, R. P.; Hilliard, L. R.; Tan, W. Surface Modification of Silica Nanoparticles to Reduce Aggregation and Nonspecific Binding. *Langmuir* **2006**, *22*, 4357–4362.
66. Stadtmueller, B. M.; Hill, C. P. Proteasome Activators. *Mol. Cell* **2011**, *41*, 8–19.
67. Forster, A.; Whitby, F. G.; Hill, C. P. The Pore of Activated 20S Proteasomes Has an Ordered 7-Fold Symmetric Conformation. *EMBO J.* **2003**, *22*, 4356–4364.
68. Tomko, R. J., Jr.; Hochstrasser, M. Molecular Architecture and Assembly of the Eukaryotic Proteasome. *Annu. Rev. Biochem.* **2013**, *82*, 415–445.
69. Osmulski, P. A.; Hochstrasser, M.; Gaczynska, M. A Tetrahedral Transition State at the Active Sites of the 20S Proteasome Is Coupled to Opening of the Alpha-Ring Channel. *Structure* **2009**, *17*, 1137–1147.
70. Kleijnen, M. F.; Roelofs, J.; Park, S.; Hathaway, N. A.; Glickman, M.; King, R. W.; Finley, D. Stability of the Proteasome Can Be Regulated Allosterically through Engagement of Its Proteolytic Active Sites. *Nat. Struct. Mol. Biol.* **2007**, *14*, 1180–1188.
71. Lee, J. H.; Huh, Y. M.; Jun, Y. W.; Seo, J. W.; Jang, J. T.; Song, H. T.; Kim, S.; Cho, E. J.; Yoon, H. G.; Suh, J. S.; *et al.* Artificially Engineered Magnetic Nanoparticles for Ultra-sensitive Molecular Imaging. *Nat. Med.* **2007**, *13*, 95–99.
72. Choi, H. S.; Liu, W.; Misra, P.; Tanaka, E.; Zimmer, J. P.; Itty Ipe, B.; Bawendi, M. G.; Frangioni, J. V. Renal Clearance of Quantum Dots. *Nat. Biotechnol.* **2007**, *25*, 1165–1170.
73. Xia, T.; Kovochich, M.; Liong, M.; Madler, L.; Gilbert, B.; Shi, H.; Yeh, J. I.; Zink, J. I.; Nel, A. E. Comparison of the Mechanism of Toxicity of Zinc Oxide and Cerium Oxide Nanoparticles Based on Dissolution and Oxidative Stress Properties. *ACS Nano* **2008**, *2*, 2121–2134.
74. Kocbek, P.; Teskac, K.; Kreft, M. E.; Kristl, J. Toxicological Aspects of Long-Term Treatment of Keratinocytes with ZnO and TiO_2 Nanoparticles. *Small* **2010**, *6*, 1908–1917.
75. Pisanic, T. R., II; Blackwell, J. D.; Shubayev, V. I.; Finones, R. R.; Jin, S. Nanotoxicity of Iron Oxide Nanoparticle Internalization in Growing Neurons. *Biomaterials* **2007**, *28*, 2572–2581.
76. Berkers, C. R.; Verdoes, M.; Lichtman, E.; Fiebiger, E.; Kessler, B. M.; Anderson, K. C.; Ploegh, H. L.; Ovaa, H.; Galardy, P. J. Activity Probe for *In Vivo* Profiling of the Specificity of Proteasome Inhibitor Bortezomib. *Nat Methods.* **2005**, *2*, 357–362.
77. Park, J.; An, K.; Hwang, Y.; Park, J. G.; Noh, H. J.; Kim, J. Y.; Park, J. H.; Hwang, N. M.; Hyeon, T. Ultra-Large-Scale Syntheses of Monodisperse Nanocrystals. *Nat. Mater.* **2004**, *3*, 891–895.